Journal of Thermal Science Vol.17, No.1 (2008) 07–20

DOI:10.1007/s11630-008-0007-z **Article ID: 1003-2169(2008)01-0007-14**

A Quasi-One-Dimensional CFD Model for Multistage Turbomachines

Olivier Léonard and Olivier Adam

University of Liège - Turbomachinery Group, Liege, Belgium
o.leonard@ulg.ac.be

The objective of this paper is to present a fast and reliable CFD model that is able to simulate stationary and transient operations of multistage compressors and turbines. This analysis tool is based on an adapted version of the Euler equations solved by a time-marching, finite-volume method. The Euler equations have been extended by including source terms expressing the blade-flow interactions. These source terms are determined using the velocity triangles and a row-by-row representation of the blading at mid-span. The losses and deviations undergone by the fluid across each blade row are supplied by correlations. The resulting flow solver is a performance prediction tool based only on the machine geometry, offering the possibility of exploring the entire characteristic map of a multistage compressor or turbine. Its efficiency in terms of CPU time makes it possible to couple it to an optimization algorithm or to a gas turbine performance tool. Different test-cases are presented for which the calculated characteristic maps are compared to experimental ones.

Keywords: multistage, compressors, turbines, quasi-one-dimensional, meanline analysis

Introduction

The performances of a turbomachine must be analyzed before it is tested on the bench or as a part of a gas turbine engine. This study provides the designer with guidelines for the choice of many design parameters and for the optimization of the configuration of the machine. It also allows to test (in a virtual way) its operation during critical manoeuvres such as startup, shutdown or load change phases which bring on important variations of mass flow or rotation speed. This exploration phase is based on the numerical modelling of the operation of the turbomachine.

The present project aims at the development of an analysis tool which can simulate the operation of the compressor or the turbine. It has to be fast enough to allow its use inside a design optimization process or inside an engine cycle deck. It has also to be sufficiently accurate and robust to bear an industrial use.

Current analysis tools, whether they are analytical [1]. or one-dimensional [2,3], are often based upon single-stage or full characteristic maps of the turbomachine. These maps are often inaccurate or simply not available, and their use is not compatible with the exploratory aspect of the simulation [2]. To solve this issue, a meanline performance prediction method is proposed in the present contribution, coupled to a quasi-one-dimensional flow solver.

This simulation tool is based on mass, momentum and energy balances applied to a one-dimensional discretization of the multistage turbomachine flowpath, and a meanline definition of the blade angles, blade row per blade row. The resolution of these equations brings a detailed description of the flow while minimizing the amount of empirical information and eliminating the need for characteristic curves. The model formulation is very general and allows the implementation of physical phenomena such as bleeds, heat transfers, cooling flows, water ingestion, fouling...

The flow path is discretized in the streamwise direc-

Received: September, 2007
Olivier Leonard: Professor

Nomenclature

Symbols

b	flowpath local height	β	relative flow angle	
CR	channel contraction ratio	δ	deviation	
E	specific internal energy	$\delta*$	boundary layer displacement thickness	
$\mathbf{F}$	conservative flux vector	ϕ	blade camber angle	
F_b	blade force	λ	local streamline angle	
H	specific enthalpy	ρ	density	
i	incidence	ζ	total enthalpy deficit coefficient	
o	blade channel throat	σ	cascade solidity	
P	static pressure	Ω	rotation speed	
$\mathbf{Q}$	source term vector	ϖ	loss coefficient	
q_m	mass flow	**Subscripts**		
r	radius	m	meridional	directions/components
s	entropy	x	axial	
S	flowpath cross-section	n	normal	
t	time / blade pitch	r	radial	
TC	blade tip clearance	θ	tangential	
$\mathbf{U}$	conservative variable vector	t	throat condition	
U	tangential rotation speed	1	blade leading edge	
V	absolute velocity	2	blade trailing edge	
Vol	blade row volume	∞	blade row reference direction	
W	relative velocity	**Superscripts**		
α	absolute flow angle	0	total condition	
		*	minimum-loss condition	

tion only, with several elementary cells in each blade row or between blade rows. The equations of mass, momentum and energy are discretized on this mesh and integrated with state-of-the-art CFD techniques. Various source terms are added to account for the physical phenomena. Losses and deviations are obtained from empirical correlations. This approach confers the method with a wide range of application, in the predictive or analysis fields.

This analysis tool was applied to a three-stage axial compressor with non-standard profiles, requiring a tuning of the correlations for losses and deviations, and to a two-stage turbine featuring multiple coolant flow injections.

Model description

Most of the fast models used for the description of the flows through a compressor or a turbine make use of single-stage characteristic maps. These maps must be user-supplied or extrapolated from previous design, which limits the application of these models as predictive tools [4]. Moreover, characteristics maps are established through expensive rig tests and cover only a part of the operational domain of the machine. Davis proposed a generation of individual stage maps from the compressor geometry [5]. These pseudo-experimental data are then used in combination with a classical 1D analysis code. This technique lacks flexibility and is also an additional, time-consuming layer in the simulation. Some methods seem more attractive, as they make use of the turbomachine geometry to estimate the velocity triangles at mid-span, on each blade row. Empirical information is introduced into the model through correlations describing the losses and deviations in the blade row [6,7].

The tool had to be fast, because of the possible unsteady aspect and the intensive use needed to draw a complete characteristic map. Throughflow 2D and full 3D simulations were left apart. The streamline curvature algorithms were also avoided, as one of the goals of this project was to allow the simulation of stalled or reversed flows. On the other hand, over-simplified models do not offer the versatility of finite-volume solvers. Analytical and lumped-volume 0-D models [1,7,8] may simulate a wide range of operating conditions but their extension to physical or technological effects is difficult.

In the present contribution it was postulated that the characteristic maps were *a priori* unknown. The model describes the flow along the meanline of the turbomachine, provided that the flowpath geometry and the blade angles at mid-span are known. The model is based upon the unsteady quasi-1D Euler equations for mass,

meridional momentum and energy balances, completed by a tangential momentum conservation equation. These equations are expressed in a general curvilinear coordinate system, allowing for radial shifts. The angular derivatives are considered to be negligible and the flow is supposed to be axisymmetric. In the frame of the quasi-one-dimensional formalism, all quantities are supposed to be constant in a cross-sectional area of the flowpath, and the working fluid is treated as an ideal gas.

Additional source terms describe the physics of the flow through the turbomachine. Velocity triangles at mid-span are determined with the help of empirical correlations and provide the source terms associated to the action of the blade rows.

Model equations

General formulation

Mass, momentum and energy conservation principles are applied to an elementary control volume (figure 1) within a curvilinear (m, n, θ) coordinate system in order to set up the quasi-1D curvilinear Euler equations.

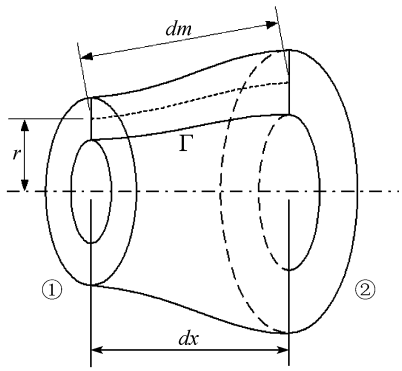

Fig. 1 Elementary control volume

The upper and lower boundaries of the control volume Γ are solid walls, while the annular surfaces 1 and 2 are porous boundaries. Mass and energy balances write:

$$\frac{\partial\, \rho S}{\partial t}+\frac{\partial\, \rho V_m S}{\partial m}=0 \tag{1}$$

$$\frac{\partial\, \rho e^0 S}{\partial t}+\frac{\partial\, \rho V_m h^0 S}{\partial m}=0 \tag{2}$$

Similarly, the momentum balance equation in the meridional direction results in the following expression, where it is accounted for a possible centrifugal force projection:

$$\frac{\partial\, \rho V_m S}{\partial t}+\frac{\partial\, (p+\rho V_m^2)S}{\partial m}= p\frac{\partial S}{\partial m}+\frac{\rho V_\theta^2 S}{r}\frac{\partial r}{\partial m} \tag{3}$$

Finally, expressing the angular momentum balance within Γ yields:

$$\frac{\partial\, \rho V_\theta S}{\partial t}+\frac{\partial\, \rho V_m V_\theta S}{\partial m}=-\frac{\rho V_m V_\theta S}{r}\frac{\partial r}{\partial m} \tag{4}$$

In vector, non-dimensional, conservative form, these equations are written as

$$\frac{\partial \mathbf{U}}{\partial t}+\frac{\partial \mathbf{F}}{\partial m}=\mathbf{Q} \tag{5}$$

$$\mathbf{U}=\begin{bmatrix}\rho S\\ \rho V_m S\\ \rho V_\theta S\\ \rho e^\circ S\end{bmatrix} \qquad \mathbf{F}=\begin{bmatrix}\rho V_m S\\ (p+\rho V_m^2)S\\ \rho V_m V_\theta S\\ \rho V_m h^\circ S\end{bmatrix} \tag{6}$$

The cross-sectional area is computed perpendicularly to the meanline, so that it takes the simple form (see figure 2 for notations):

$$S=2\pi\cdot r\cdot b$$

The mass flow corresponds to the second conservative variable:

$$q_m=\rho\cdot V_m\cdot S$$

The system of equations (5) describes the evolution of the fluid through any type of machine, axial, radial or mixed-flow, provided that the appropriate source terms are supplied to the model. It is assumed that the flowpath meanline is a streamline, and that the flow is axisymmetric. In case of a pure axial flow (as in the first application described hereafter) the conversion from curvilinear to cylindrical coordinates only requires the meridional subscript m to be replaced by the axial one x.

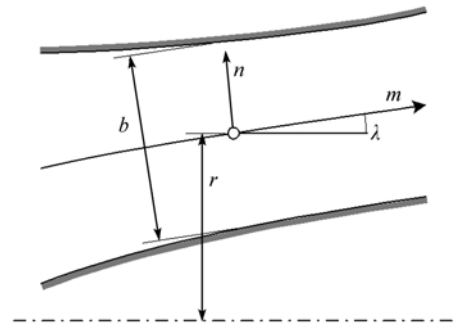

Fig. 2 Curvilinear coordinate system

This quasi-1D system of equations can also be deduced from the streamtube curvilinear equations [9], noting that the velocity normal to the streamsurface is neglected in the quasi-1D formalism. The normal curvature k_n can be written in function of the streamtube height b; the meanline data yield immediately the streamline angle λ:

$$k_n=\frac{1}{b}\frac{\partial b}{\partial m} \qquad \sin\lambda=\frac{\partial r}{\partial m}$$

In (5), **Q** is the vector of source terms. It is divided into four distinct contributions, categorized according to their physical meaning:

$$\mathbf{Q} = \mathbf{Q}_b + \mathbf{Q}_f + \mathbf{Q}_g + \mathbf{Q}_c \tag{7}$$

These successive contributions model the effects of work or heat exchange undergone by the fluid through the turbomachine. Namely, they stand for

- b : inviscid blade force
- f : viscous force
- g : forces due to area or radius variations
- c : cooling source terms

The source term vector **Q** depends on the velocity triangles. Its evaluation is described hereafter.

Velocity triangles

The solver is based on a time-marching procedure and at each time step, the velocity triangles are drawn at the mid-span on each blade row. The predictive capability of the analysis tool is derived fundamentally from this process.

Starting from the blade geometry at mid-span, the conservative variables of the current solution are combined with empirical information brought by correlations to determine the velocity triangles. The blade material angles are known at the leading and trailing edges, as are the fluid angles and velocity at the blade leading edge.

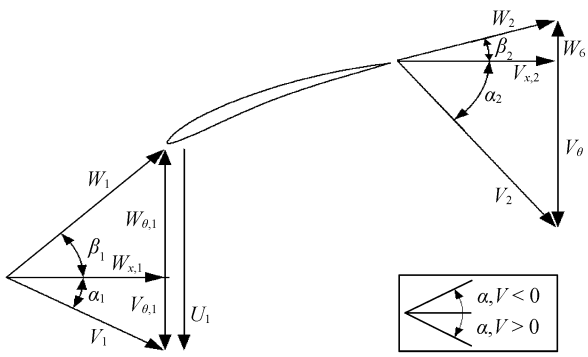

Fig. 3 Velocity triangles for a compressor blade

The accuracy of the simulation is tightly related to the adequacy of the losses and deviation correlations with the type of blades. This is particularly true for compressors. Each manufacturer has its own, confidential, correlations, and it is often difficult to render the operation of a modern compressor by means of the correlations available in the open literature. Tuning parameters have therefore been integrated into standard correlations.

For compressors, the NASA method is used to evaluate the reference minimum-loss incidence, and the reference deviation is given by Carter's rule [10]:

$$i^* = K_{sh} \cdot K_{t,i} \cdot (i_0)_{10} + n \cdot \phi \tag{8}$$

$$\delta^* = \frac{m\phi}{\sqrt{\sigma}} \tag{9}$$

The shape, thickness and camber coefficients, as well as the zero-camber incidence angle, have been fitted from the NASA data.

The off-design deviation correlation is the one from Creveling [11]. It has been chosen for its good performance on a wide range of profiles [12, 13]:

$$\frac{\delta - \delta^*}{\Delta\beta^*} = f\left(\frac{i - i^*}{\Delta\beta^*}\right) \tag{10}$$

The function f has been fitted from experimental data by two quadratic functions.

The blade row flow angles and mass flow are known from the previous evaluations. The meridional velocity at the blade row exit is iterated until these conditions are matched.

The reference loss coefficient is evaluated through the classical correlation of Koch and Smith [14]. This very complete correlation includes a large number of physical parameters and has proven to produce accurate results.

The off-design profile loss coefficient, when using the standard open-literature correlations, is deduced from the results of Creveling [11]:

$$\varpi - \varpi^* = c_m \cdot (i - i^*)^2 \tag{11}$$

In reason of its particular shape, the coefficient c_m has been fitted by a Chebyshev polynomial approximation. This same curve can be tuned through optimization parameters if needed.

An additional loss coefficient contribution renders the complex loss mechanisms associated with the secondary flows. It is based on a simple relationship, suggested by Howell [15] and still widely used [16,17]:

$$\varpi_s = 0.018 \cdot C_L^2 \cdot \sigma \cdot \frac{\cos^2 \beta_1}{\cos^3 \beta_\infty} \tag{12}$$

The lift coefficient is estimated through the velocity triangles.

Although the system of equations (5) describes a mean flow for the whole compressor channel height, spanwise variations of losses and deviations must be included in the simulation to achieve certain trustworthiness.

Wall effects for rotors and stators, such as flow overturning or tip clearance, have been introduced into the correlations in the form of loss coefficient and deviation corrections. According to Roberts *et al.* [18] parametric spanwise curves have been averaged along the blade height to obtain mean contributions, which depend on operational parameters like end-wall boundary layer displacement thicknesses, blade camber and solidity, channel aspect ratio, or wheel tip clearance.

A sample spanwise curve, as described by Roberts *et*

al, is presented in figure 4 for a rotor. This graph represents the variations of the local deviation angle from the 2D value, predicted by the correlations based on the blade element theory.

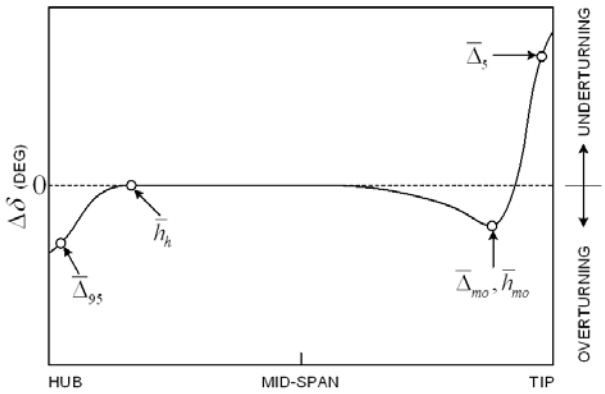

Fig. 4 Spanwise variation of rotor deviation

Assuming a "standard" meridional velocity distribution represented in figure 5, the loss and deviation curves proposed by Roberts *et al*, for rotors and stators, have been integrated using the meridional velocity as a weighting factor.

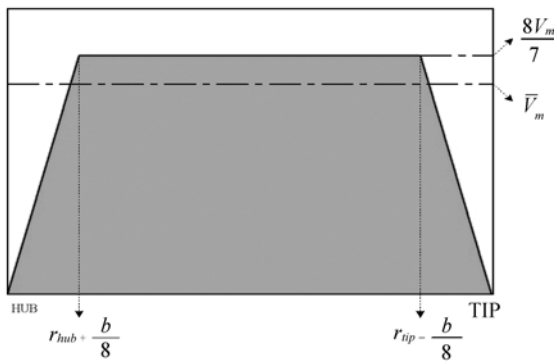

Fig. 5 Normalized meridional velocity distribution

The maximum level of meridional velocity has been set up according to:

$$\int_{r_{hub}}^{r_{tip}} V_m \, dr = \frac{7b}{8} V_{\max} = \overline{V}_m \, b \tag{13}$$

The spanwise variations have been fitted using connected straight lines. For the deviation variation of figure 4, the correction is averaged using equation (14).

$$\frac{\int_{r_{hub}}^{r_{tip}} \Delta\delta \, V_m r dr}{\int_{r_{hub}}^{r_{tip}} V_m r dr} = f\left(\delta^*, \phi, \sigma, \frac{b}{c}, TC\right) \tag{14}$$

According to this piecewise discretization, the numerator and the denominator reduce to a sum of integrals performed with the help of a symbolic solver.

The remaining expressions of loss and deviation corrections for rotors and stators have been derived similarly, yielding a complete functional correlation for 3D effects. The required boundary layer displacement thicknesses originate from the end-wall boundary layer model, as will be shown later.

For turbines, the convergent-divergent configuration of the blade channel leaves less room for variations around the blade trailing edge material angle. The Ainley-Mathieson [19] outlet flow angle correlation is therefore still widely used among the turbine performance codes. This correlation estimates a base subsonic angle at the trailing edge of the turbine blade, using the "gauge rule", then corrects it for a potential curvature of the upper surface of the blade profile between the passage throat and the trailing edge.

$$\beta_{2,LS} = 11 - 1.15083 \cdot \arccos\left(\frac{o}{t}\right) - 4\frac{t}{r_{SS}} \tag{15}$$

If a supersonic outlet Mach number is observed, a choked flow angle can be written as

$$\beta_{2,choke} = -\arccos\left(\frac{S_t}{S_2}\right) \tag{16}$$

For historical reasons, there is less standardization and parameterization among the turbine blade profiles than for the compressors. The turbine profile families are rare, and the sections are often published as a series of coordinates. Specific tools were therefore written to extract the geometrical parameters needed by the correlations. The blade row throat, the mean suction surface curvature radius, the blade backbone and the channel throat area were all numerically computed from the suction and pressure surface curves. The contraction ratio *CR* is defined as the ratio of the largest circular arc length that can be drawn inside the inlet blade-to-blade channel to the geometrical throat, which is the minimal distance between two adjacent blades. It is used for loss correlations. When dealing with loss or deviation correlations, the blade material angles at the leading and trailing edges are almost always required. According to the definition of the camberline of a blade, circles were fitted into the profiles: the camberline is simply the locus of the circle centers. Its leading and trailing edge slopes yield the blade material angles, and the camberline length is the blade backbone (Figure 6).

According to the blade row exit Mach number, the expressions (15), (16) or a blend of both, can be used:

$$\begin{cases} M_2 \leqslant 0.5 & \Rightarrow \beta_2 = \beta_{2,LS} \\ 0.5 < M_2 < 1 & \Rightarrow \beta_2 = f\left(\beta_{2,LS}, \beta_{2,choke}\right) \\ M_2 \geqslant 1 & \Rightarrow \beta_2 = \beta_{2,choke} \end{cases}$$

A tip clearance correction for the meanline outlet flow angle was proposed by Ainley and Mathieson in [20] and applied in [19]; it is used in the model.

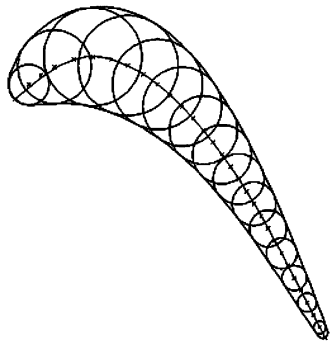

Fig. 6 Turbine blade camberline extraction

The correlations should be chosen according to the type of blade profiles, especially those for total pressure primary losses and for the deviations. For turbine blades there are no profile families with corresponding correlations. The chosen set of correlations should therefore be optimized for some test cases to show the real capabilities of the model. The lack of validation data prevented this tuning phase.

A limited number of correlations for total pressure losses undergone by the fluid in a turbine blade row are available in the open literature. The correlation proposed by Ainley and Mathieson is quite outdated and seems to overpredict the losses for most of the modern turbine profiles. However, it models all the loss components for both design and off-design conditions; it was thus included in the model. The well-known Dunham-Came [21] correlation modified Ainley and Mathieson's according to more recent turbine data and better understanding of some aspects of the flow, as the secondary losses. It represents a small correction to the AM correlation and is also presented in the model.

Kacker and Okapuu [22] also started from the AM correlation, trying to improve the design-point loss prediction. It therefore has to be completed by an off-design loss correlation. Zhu and Sjolander [23] proposed a coherent set of correlations based on a somewhat modified KO design point profile loss correlation, intended for use with the Benner et al. [24] off-design correlation. Matching secondary losses may then be computed through an original correlation due to the same authors [25,26]. The latter implies the blade row inlet boundary layer displacement thickness. Dunham [27] indeed underlined that the secondary losses may be strongly affected by the upstream wall boundary layer, and recalled the need for a boundary layer model for turbines, similar to Stratford's model [28] for compressors. Unfortunately, very few papers have addressed this question, at least as far as turbine meanline predictions are concerned. It seems unlikely to set up a reliable boundary layer displacement thickness model in the frame of a meanline turbine analysis, because the wall boundary layer is actually removed by each blade row and injected into the mainstream as a vortex core [27]. Moreover, the Benner et al. secondary loss correlation is based upon turbine cascade test results and it cannot be used to predict engine-level losses without some general scaling factor [26]. The KO-Benner correlation was then left apart.

The Craig and Cox correlations [29] were also incorporated into the model. Not as widely used as the AM loss model, it is however very complete. It was based on numerous tests on cascades, turbines and also casings. Craig and Cox showed that their method was able to predict the performance of actual machines over a wide range of Reynolds numbers, Mach numbers, aspect ratios and other relevant variables with good accuracy. The main advantage of this loss correlation is that it does not represent cascade test results; it is considered to predict radially averaged losses that may directly be used for turbine meanline performance estimation [30]. All graphical relationships were converted to analytical functions, making it possible to use the complete loss prediction inside the quasi-1D simulation tool. To briefly describe it, the Craig and Cox correlation computes the total enthalpy deficit coefficient as the combined contributions of profile, secondary and annulus losses:

$$\zeta_{tot} = \zeta_p + \zeta_s + \zeta_a \tag{17}$$

The profile loss coefficient is decomposed into several contributions and scaling factors:

$$\begin{aligned}\zeta_p = {} & \chi_R \cdot \chi_{Te} \cdot \chi_i \cdot \zeta_{p,0} \\ & + \Delta\zeta_{p,M} + \Delta\zeta_{p,Se} + \Delta\zeta_{p,Te}\end{aligned} \tag{18}$$

The first term of (18) represents the profile loss for subsonic flow at the incidence where the loss is the minimum. It is correlated with the fluid inlet angle at minimum-loss incidence, the contraction ratio *CR* and the outlet flow angle. The minimum-loss incidence itself is a function of positive and negative stalling incidences, which in turn depend on the blade inlet angle, the blade contraction ratio, the pitch to backbone length and throat to pitch ratios. The base profile coefficient is corrected by three coefficients for the Reynolds number, for the trailing edge thickness and for the incidence variation with respect to the minimum-loss incidence.

Finally, three loss increments are added to the profile losses: one for the outlet isentropic Mach number influence, one for a possible non-null suction side trailing edge curvature, and one for the trailing edge thickness effect.

Blade force source term

The forces applied by the blades onto the fluid can be deduced from the knowledge of the velocity triangles. An angular momentum balance over the blade row provides the tangential component of the blade force:

$$rF_{b\theta} = \frac{q_m}{\mathrm{Vol}}\left(r_2 V_{\theta 2} - r_1 V_{\theta 1}\right) \tag{19}$$

In the case of a rotor, this force is responsible for the shaft work:

$$SW = \Omega r F_{b\theta} \tag{20}$$

It is considered that the force exerted by the blade on the fluid is applied in an isentropic way, the viscous contribution being applied separately through a friction source term. The blade force is therefore supposed to be perpendicular to the local relative speed:

$$\vec{F}_b \cdot \vec{W} = 0 \tag{21}$$

The meridional component yields:

$$F_{bm} = -F_{b\theta}\frac{W_\theta}{V_x} \tag{22}$$

Equations (19) and (22) fully define the inviscid blade force source term:

$$\mathbf{Q}_b = \begin{bmatrix} 0 \\ F_{bm}\, S \\ F_{b\theta}\, S \\ F_{b\theta}\, \Omega r S \end{bmatrix} \tag{23}$$

Friction source term

As the blade force application is isentropic, the entropy modification is devoted to a separate viscous force, according to a distributed loss model such as proposed in [31]. The magnitude of the dissipative force is related to the entropy creation along a streamline using the definition of the rothalpy and the Gibbs relation [32]:

$$\left|\vec{F}_f\right| = \rho T \frac{V_m}{W}\frac{\partial s}{\partial m} \tag{24}$$

The entropy gradient arises directly from the combined loss coefficient. The dissipative force is aligned with the relative speed vector, with an opposite direction, resulting in:

$$\vec{F}_f = -\left|\vec{F}_f\right|\frac{\vec{W}}{\left|\vec{W}\right|} \tag{25}$$

Once again, only the tangential component of the force is likely to modify the energy balance. Equations (24) and (25) can be used to determine the complete friction source term:

$$\mathbf{Q}_f = \begin{bmatrix} 0 \\ F_{fm}\, S \\ F_{f\theta}\, S \\ F_{f\theta}\, \Omega r S \end{bmatrix} \tag{26}$$

Geometrical source term

This source term gathers the contributions of the flowpath geometry to the equations, namely the cross-sectional area and the meanline radius variations. In a way similar to the inviscid blade force, it is interesting to notice that the right hand side expression of the angular momentum equation (4) may be interpreted as a volumic force which is such that the centrifugal force source term present in the meridional momentum equation (3) does not create entropy. The corresponding force is indeed perpendicular to the velocity vector:

$$F_{km} = \frac{\rho V_\theta^2}{r}\frac{\partial r}{\partial m}$$

$$F_{k\theta} = -\frac{\rho V_m V_\theta}{r}\frac{\partial r}{\partial m}$$

Only the tangential component participates in the energy balance. The final form of the geometrical source term is

$$\mathbf{Q}_g = \begin{bmatrix} 0 \\ F_{km} S + p\dfrac{\partial S}{\partial m} \\ F_{k\theta}\, S \\ 0 \end{bmatrix} \tag{27}$$

Cooling source term

In case of stationary operation of turbines, the only heat exchange is due to cooling flows which can be injected in the turbine flowpath, either between the blade rows or through the blade walls. In any case it will be considered here that the cooling flows do not participate in the meridional or angular momentum balances.

Figure 7 shows an example of cooling mass flows and how they are laid along the turbine flowpath. These coolant injections are those observed on the Energy Efficient Engine High Pressure Turbine, which is the validation test case presented hereafter. The CFD representation of the turbine splits the blade rows into several control volumes, allowing the coolant injections to be located at the leading or trailing edge of a given blade, as this is the case for the first stator of figure 7.

The cooling source term introduces the cooling mass flow and the associated enthalpy flux into the appropriate equations.

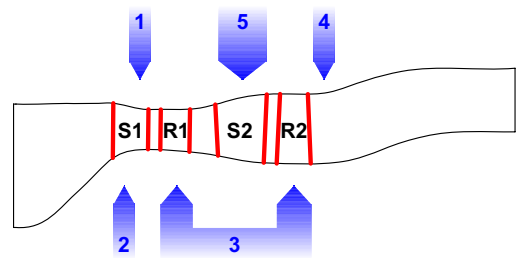

Fig. 7 Cooling mass flow location

The quantities are positive for an injection, and negative for a pumping. On a dimensional point of view, it

can be noticed that q_{cool} is a distributed mass flow.

$$\mathbf{Q}_c = \begin{bmatrix} q_{cool} \\ 0 \\ 0 \\ q_{cool}\ h^0_{cool} \end{bmatrix} \tag{28}$$

Equation solver

The quasi-1D set of Euler equations is made up of expressions (5), (6), (23), (26), (27) and (28). It describes a two-dimensional flow, developing on an axisymmetric flow surface generated by the revolution of the turbine meanline around the rotation axis.

The one-dimensional discretization of the computation domain takes into account the curvilinear frame of reference. It can be seen on the example of figure 8 that the blade rows are divided internally into control volumes, in order to obtain moderate flow deflections for each elementary cell (a real mesh holds actually more computing cells than shown hereunder). This is convenient for compressors and is necessary for turbine computations, because of the large fluid deflections observed in the turbine blade rows. This internal blade division can be used to concentrate the cooling mass flows.

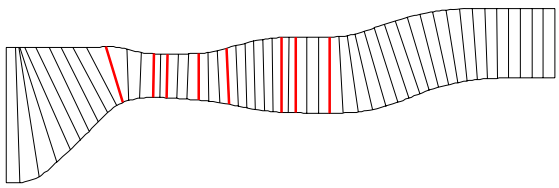

Fig. 8 Quasi-one-dimensional mesh

The integral form of the Euler system of equations is written for each cell. The flow solver relies on the upwind discretization of the fluxes proposed by Roe to ensure a good stability of the computation. The quadratic, limited, hybrid reconstruction scheme [33] was used. The solver is ready for unsteady computations, provide that appropriate transient heat exchange source terms are introduced.

For a steady-state simulation, a time-marching solver allows the system to evolve toward a stationary solution. The boundary conditions applied at the inlet and outlet of the compressor, for an unstalled forward flow, are listed in table 1.

Table 1 Boundary conditions

	Inlet	outlet
imposed	$p^{\circ}_{in}, T^{\circ}_{in}, \alpha_{in}$	p_{out}

An implicit time integration scheme is used to cope with the strong source terms. In stationary mode, this implicit scheme works with an Euler single-step forward time differentiation. At each time step, several sub-iterations are necessary to ensure a smooth convergence of the simulation. The time differentiation of (5) yields:

$$\mathbf{F}(\mathbf{U}^{n+1}) = \frac{\mathbf{U}^{n+1} - \mathbf{U}^{n}}{\Delta t} - \mathrm{RHS}\left(\mathbf{U}^{n+1}\right) = 0 \tag{29}$$

Linearizing equation (29) yields

$$\begin{aligned} \mathbf{F}(\mathbf{U}^{n+1}) &= \mathbf{F}(\mathbf{U}^{n}) + \mathbf{J}\cdot(\mathbf{U}^{n+1} - \mathbf{U}^{n}) \\ &= -\mathrm{RHS}\left(\mathbf{U}^{n}\right) + \mathbf{J}\cdot(\mathbf{U}^{n+1} - \mathbf{U}^{n}) \end{aligned} \tag{30}$$

A smart node-coloring finite-difference scheme defines the Jacobian matrix. It takes advantage of the reconstruction method and of the mesh structured aspect to limit the computational burden.

$$\mathbf{J}_{i,j} \approx \frac{\mathbf{F}_i\left(\mathbf{U}^n_j + \delta\mathbf{U}^n_j\right) - \mathbf{F}_i\left(\mathbf{U}^n_j\right)}{\delta\mathbf{U}^n_j} \tag{31}$$

The linearized system (30) becomes

$$\mathbf{J}\cdot\delta\mathbf{U} = \mathrm{RHS}\left(\mathbf{U}^{n}\right) \tag{32}$$

Because of the first-order Taylor expansion lying under this expression, several updates of the conservative variables may be necessary to compute an accurate flow evolution between two successive time steps. This is the case for the turbine simulation, which has shown to bring on steep and spatially concentrated source terms.

Due to its fairly small size, the system (32) is solved directly through a simple LU decomposition. It could be treated more efficiently but the block-penta-diagonal aspect of the Jacobian matrix would require a very specific development. The resulting computer code requires a few seconds CPU time to simulate the operation of a multistage turbomachine.

Annulus boundary layer model

A realistic model for multistage compressors requires the simulation of the annulus boundary layers. The simple model proposed by Stratford [28] has been selected. The Stratford model solves momentum balance across the successive blade rows of the compressor. The boundary layer shape factor and skin friction are roughly estimated. The force defect is assumed to be zero and the boundary layer flow is supposed collateral. These approximations yield a fair estimate of meridional blockage [34].

The blockage due to end-wall boundary layers is integrated into the cross-sectional areas appearing in the quasi-1.5D Euler equations (5). Besides, the loss model of Roberts *et al* uses the displacement thickness to predict the losses associated with the end-wall boundary layers and tip clearances.

The annulus boundary model is applied at each time

step, based on the current solution. The implicit scheme does not integrate it into the Jacobian matrix estimation to limit the computation effort.

Three-stage axial compressor

The compressor chosen as a first validation example is a test model of the last three stages of a bigger eight-stage compressor [35], subsequently named PW3S1. The flow path is characterized by a constant mean radius, and a constant cross-sectional area (figure 9). The real mesh would fail to clearly show the cell distribution, since it contains about 200 control volumes.

Fig. 9 PW3S1 compressor flow path mesh

This compressor is composed of an inlet guide vane and three rotor-stator stages. The blade profiles are based on a NACA65 thickness distribution over a circular camberline. As expected, the standard correlations are not adapted to this type of blades and the first results are not satisfactory, as figure 10 shows for the nominal rotation speed. The results are particularly disappointing at reduced mass flow. The predicted deviation angles are too low, which results in an over-estimated pressure ratio, and also in too high predicted mass flows in the same zone. Figure 11 illustrates the efficiency prediction, showing only a constant offset that can easily be compensated by tuning the secondary losses equation.

Consequently, a parametric identification procedure has been conducted to demonstrate the generalization capabilities of the analysis tool, named Quads in the following. The objective of this procedure is to identify some parameters introduced in the standard correlations, on the sole basis of the 100% nominal speed data. It is hoped that the modified loss and deviation models will be able to provide a good solution in an extended range of mass flows and rotation speeds. The choice of optimization parameters is explained hereafter.

Figure 10 suggests that the reference incidence, deviation and primary loss coefficient are fairly well defined by the standard correlations. Some tuning coefficients are introduced into the off-design deviation angle and primary loss correlations. The formulation of Creveling, equation (10), has been kept for the off-design deviation angle. But the expression of the function f has been replaced by two cubic polynomials that match at (0,0):

$$x = \frac{i - i^*}{\Delta\beta^*} \tag{33}$$

$$\begin{cases} x > 0 \rightarrow f_{(x)} = c_{3p}x^3 + c_{2p}x^2 + c_{1p}x \\ x < 0 \rightarrow f_{(x)} = c_{3n}x^3 + c_{2n}x^2 + c_{1n}x \end{cases} \tag{34}$$

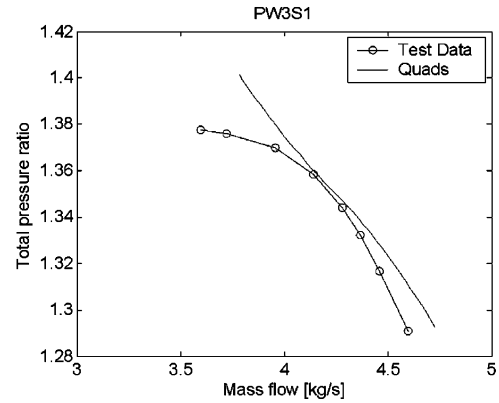

Fig. 10 "Standard correlations" pressure line

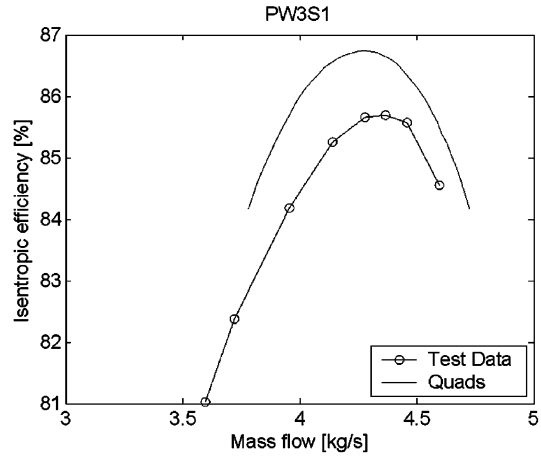

Fig. 11 "Standard correlations" efficiency line

The primary loss coefficient also keeps the form used in Creveling's relation (11). However, the numerous simulations conducted on the PW3S1 compressor show that the relative Mach number is almost constant over the considered operation interval, at nominal rotation speed. It was decided to introduce only two parameters in the expression of the off-design primary loss coefficient:

$$\begin{cases} i > i^* \rightarrow \varpi - \varpi^* = c_{mp} \cdot (i - i^*)^2 \\ i < i^* \rightarrow \varpi - \varpi^* = c_{mn} \cdot (i - i^*)^2 \end{cases} \tag{35}$$

The boundary layer thickness at the compressor inlet is not specified in the published test data [36] and it is therefore included in the set of optimization coefficients. A unique coefficient is introduced into the annulus boundary layer model. It represents the ratio of the wall boundary layer thickness to the channel height, at the

inlet of the compressor.

Finally, a tuning coefficient is added to the secondary losses equation, in order to compensate for the offset efficiencies (figure 11):

$$\varpi_s = k_{sl} \cdot C_L^2 \cdot \sigma \cdot \frac{\cos^2 \beta_1}{\cos^3 \beta_\infty} \tag{36}$$

The parametric identification problem has been solved using a Nelder-Mead optimization algorithm, which is a 0-order method that does not need the objective function derivatives. The algorithm was chosen because of its good global minimum finding capabilities and the linearly increasing computational burden with the number of variables. The objective function was defined as a weighted sum of the relative errors on the predicted mass flow, pressure ratio and efficiency. This optimization procedure has been made possible thanks to the reduced execution time of the analysis tool. After reaching an acceptable solution, the optimized correlations permit a close prediction of the PW3S1 compressor performance at 100% nominal speed. These correlations were used to simulate the whole compressor map. The results are shown in figures 12 and 13. The 85%NN and 105%NN operating curves show the good generalization capabilities of the optimized correlations, for the pressure ratio as well as for the isentropic efficiency. The adapted off-design deviation angle correlation correctly renders the pressure ratio collapsing at low mass flows. On the other hand, at high mass flows, the deviation angle correlation of Creveling also had to be modified to match the experimental data. Once again, at high mass flow and rotation speed, the annulus boundary layer model fails to correctly represent the increasing blockage and subsequent mass flow reduction.

The predicted mass flow is also slightly too high for the whole 105%NN pressure line, denoting the same problem of a perfectible end-wall boundary layer model.

Figure 13 shows that the global loss level has been adjusted. The predicted efficiency curves closely match the measured data. It could be interesting to explore the dependency of the c_{mp} and c_{mn} coefficients of equation (35) to the Mach number level. This could not be captured on a single operating line. It would have needed an optimization process based on several curves, which was not the point demonstrated here. However, the peak efficiency is correctly predicted for the three rotation speeds, despite the rough primary loss correlation.

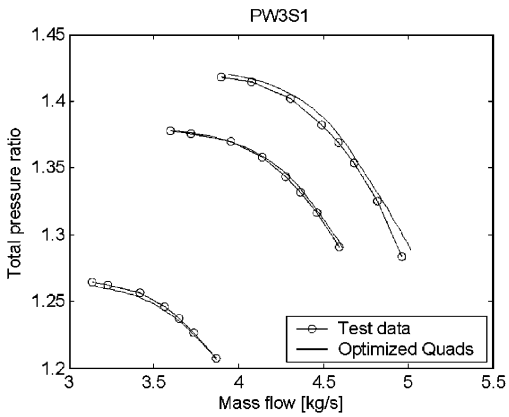

Fig. 12 "Optimized correlations" pressure lines

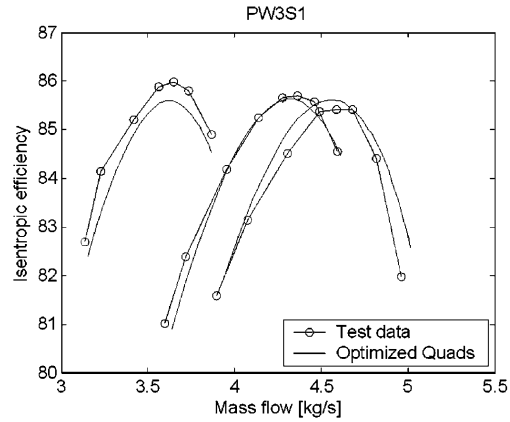

Fig. 13 "Optimized correlations" efficiency lines

Two-stage cooled turbine

The turbine test case is a component test originating from the Energy Efficient Engine project. The moderate loading, high-pressure turbine was run on a full scale warm air turbine test rig, with cooling flows (figure 14). Experimental data are available for a wide range of operating conditions [37].

The stator and rotor blades are described at three radial stations (hub, mid-span and casing) through series of coordinates. As already stated, these raw profiles were numerically treated to extract their useful geometric attributes; see for example figure 6.

A simplified version of the one-dimensional mesh applied to the turbine flowpath is shown in figure 8. The real mesh counts more than three hundred mesh cells and is less readable. It was found that the large deflections imposed inside the blade zones to the working fluid had to be distributed over an important number of inner blade cells to keep the truncation errors at an acceptable level. The rest of the machine was meshed accordingly to obtain a homogeneous 1D spatial discretization.

The NASA report [37] provides global data for a large number of test runs. They were obtained by varying the turbine back pressure, then sweeping a given range of rotation speed. Inlet total pressure and temperature were kept as constant as possible.

The cooling configuration is shown in figure 14. The schematic translation into the quasi-1D model and its

computational domain is shown in figure 7. The cooling mass flows were not available nor the cooling holes total cumulative area. The only specified variables of the cooling system are the inlet conditions of the coolant air. These data were set to obtain given mass flows at the design point [37]. But, as the operating point varies, so does the counter-pressure inside the turbine, and the cooling flows are expected to differ from their design values.

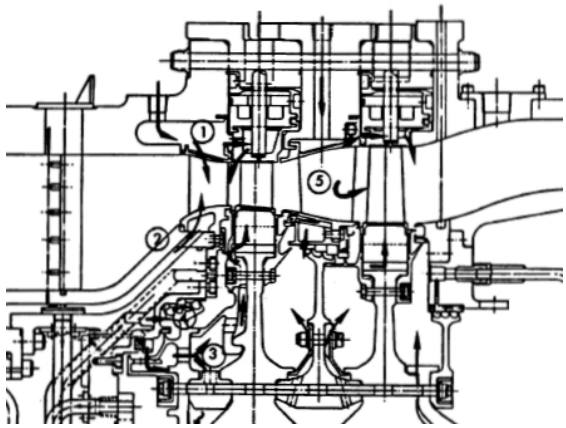

Fig. 14 EEE HPC turbine

The analysis tool Quads was run similarly to the rig test by varying the downstream static pressure and the rotation speed. The results are presented hereafter, in terms of variables used by Timko [37]: corrected speed, corrected mass flow, energy function and efficiency.

It appeared that the Craig-Cox total enthalpy loss correlation was giving the best results without any tuning. The profile and secondary losses were introduced in the velocity triangle computation: by lack of information, the annulus loss of Craig and Cox was not evaluated. The flow angles were estimated through the previously detailed Ainley-Mathieson correlation.

Figure 15 shows the total-to-total pressure ratio in function of the corrected rotation speed for a varying downstream static pressure. The back pressure values are indicated under the form of an inlet total to outlet static pressure ratio. The simulated pressure ratios are very satisfying and the flow angles are correctly predicted.

Figure 16 shows a good agreement between the predicted and measured values of the energy function. This variable describes the total enthalpy drop through the turbine, normalized by the total temperature right after the first nozzle. A detailed analysis of the results showed that this temperature was somewhat overestimated, inducing the observed discrepancies. This should be corrected by the introduction of a proper cooling loss model, and maybe a wall friction loss model.

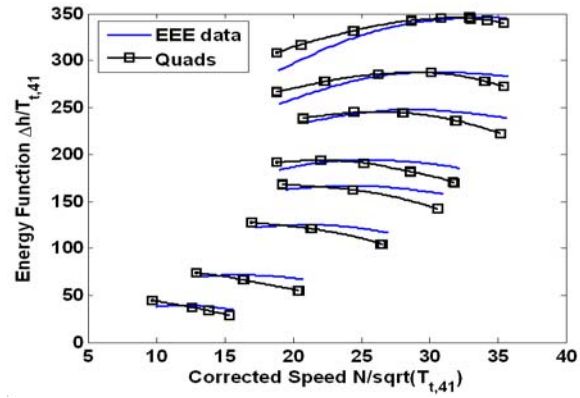

Fig. 16 Energy function vs. corrected speed

Figure 17 compares the corrected mass flows. As the mass flow is not imposed in the computation but depends highly on how the loss correlations erode the fluid energy, the results were expected to differ from the measured data. Notwithstanding these errors, one can notice that the simulation tool captures the turbine blockage which takes place at high expansion rate, as on the real turbine. The low speed, low expansion rate curves do not show

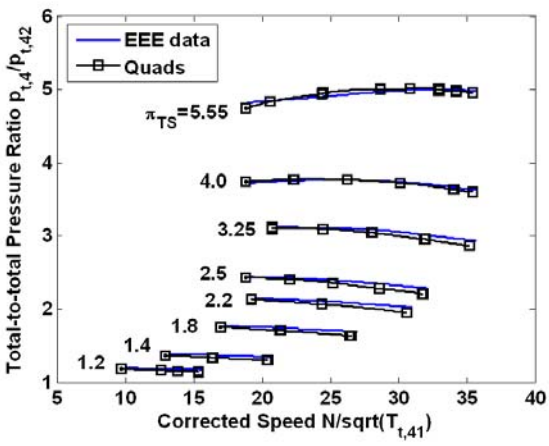

Fig. 15 Total pressure ratio vs. corrected speed

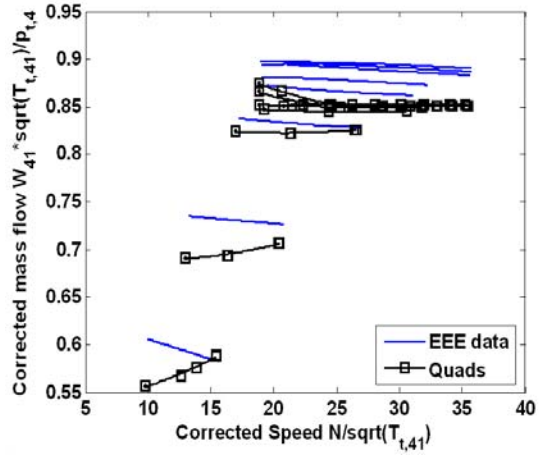

Fig. 17 Corrected mass flow vs. corrected speed

the correct trend with increasing rotation speed. This is without any doubt connected with the cooling mass flows. Their knowledge is incomplete and the loss correlations are not yet adequate. Future developments should focus on getting better understanding of the turbine mass flow evolution, in close relation with the cooling mass flows and the associated phenomena.

Finally, figure 18 compares the efficiencies obtained with standard loss correlations to those measured on the rig. To get correct extrapolation capabilities of the model towards low rotation speeds, for example, the loss correlations should at least have been optimized on one operating line, as for the compressor test-case. Turbine operation is a very complex process, depending on a great number of factors, and it is unlikely that a general correlation would give close predictions for such a particular turbine.

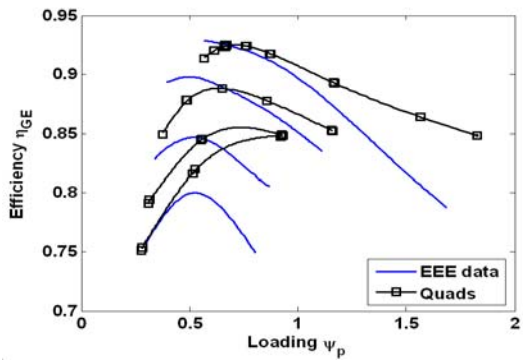

Fig. 18 Efficiency vs. loading

Despite these restrictions, figure 18 shows that the model predicts fair trends for the efficiencies, except for the lowest expansion rates.

Conclusions

A meanline model for multistage turbomachines has been presented. This analysis tool allows the exploration of the characteristic map of a multistage compressor or turbine, based on the flowpath geometry and the blade angles at mid-span. Its very low computational burden (a few seconds CPU time) makes it possible to couple it with an optimization algorithm or a gas turbine performance deck.

The correlations introducing empirical information into the simulation originate from the open literature. They can be exchanged for a manufacturer's own correlation set or they can be tuned by means of optimization coefficients. Equipped with adequate correlations, the model has shown an excellent agreement when compared to measured data.

The introduction of physical effects through source terms is a very generic approach that can be used to simulate complex configurations or phenomena such as water ingestion, blade fouling or blade wear. The model can be extended to combustion chambers [38] to simulate the operation of a whole gas turbine engine [2].

The model has a wide potential of applications, from stationary to transient, from low speed to high speed, from forward to reverse flows. Based on the unsteady Euler equations, it can indeed be extended to the simulation of slow or rapid transient phenomena such as mechanical inertia, heat soakage or pneumatic effects. In the near future, further developments will be directed towards surge detection, which appears necessary in the scope of a useful performance prediction tool [17]. The extrapolation of compressor maps to very low speeds is also planned, to study the windmilling of compressors.

The validation test case shows the possibilities of the code, but also its limitations. The predicted performances of the two-stage EEE high-pressure turbine are fairly satisfying, especially when it comes to the estimated total pressure ratio or total enthalpy drop, even though the correlations used for the validation have by no means been optimized for the EEE turbine. However, the simulated mass flow and efficiency underline the need for a cooling loss model. Subsequent development efforts will tend to introduce an one-dimensional mixing model for the evaluation of the cooling losses [39, 40].

With proper total pressure loss [41] and slip factor [42] correlations, the model could also be adapted for centrifugal compressors. The curvilinear coordinate system makes this adaptation quite straightforward.

References

[1] SELLERS J.F., DANIELE C.J., 1975: DYNGEN - A Program for Calculating Steady-State and Transient Performance of Turbojet and Turbofan Engines, NASA Technical Note TN-D-7901.

[2] REDDY K.C., NAYANI S.N., 1985: Compressor and Turbine Models - Numerical Stability and Other Aspects, AEDC Report TR-85-5.

[3] GARRARD G.D., 1995: ATEC: The Aerodynamic Turbine Engine Code for the Analysis of Transient and Dynamic Gas Turbine Engine System Operations, Ph.D. Thesis, University of Tennessee, USA.

[4] O'BRIEN W.F., 1992: Dynamic Simulation of Compressor and Gas Turbine Performance, AGARD LS-183, pp. 5.1–5.28.

[5] DAVIS M.W.Jr, 1987: A Post-Stall Compression System Modeling Technique, NASA Technical Report AD-A177610.

[6] BLOCH G.S., O'BRIEN W.F., 1992: A Wide-Range Ax-

ial-Flow Compressor Stage Compressor Model, ASME Paper 92-GT-58.

[7] SCHOBEIRI M.T., ATTIA M., LIPPKE C., 1994: GETRAN: A Generic, Modularly Structured Computer Code for Simulation of Dynamic Behaviour of Aero- and Power Generation Gas Turbine Engines, ASME Journal of Engineering for Power, Vol 116, pp. 483–494.

[8] DAY I.J., FREEMAN C., 1993: The Unstable Behaviour of Low and High Speed Compressors, ASME Paper 93-GT-26

[9] VAVRA M.H., 1960: Aero-Thermodynamics and Flow in Turbomachines, John Wiley and Sons, New-York.

[10] LIEBLEIN S., 1965: Experimental Flow in Two-Dimensional Cascades, NASA SP-36, pp. 183–226.

[11] CREVELING H.F., CARMODY R.H., 1968: Axial Flow Compressor Computer Program for Calculating Off-Design Performance (Program IV), NASA Contract Report CR-72427.

[12] ÇETIN M., ÜÇER A.Ş., HIRSCH CH., SEROVY G.K., 1987: Application of Modified Loss Correlations to Transonic Axial Compressors, AGARD Report 745.

[13] CAHILL J.E., 1997: Identification and Evaluation of Loss and Deviation Models for Use in Transonic Compressor Stage Performance Prediction, M.Sc. Thesis, Virginia Polytechnic Institute and State University, USA.

[14] KOCH C.C., SMITH L.H.Jr, 1976: Loss Sources and Magnitudes in Axial-Flow Compressors, ASME Journal of Engineering for Power, july 1976, pp. 411–424.

[15] HORLOCK J.H., 1958: Axial Flow Compressors, Butterworths Scientific Publications, London, UK.

[16] CUMPSTY N.A., 1989: Compressor Aerodynamics, Longman Scientific & Technical, Harlow, UK.

[17] AUNGIER R.H., 2003: Axial-Flow Compressors - A Strategy for Aerodynamic Design and Analysis, ASME Press, New York, USA.

[18] ROBERTS W.B., SEROVY G.K., SANDERCOCK D.M., 1986: Modeling the 3D Flow Effects on Deviation Angle for Axial Compressor Middle Stages, ASME Journal of Engineering for Gas Turbines and Power, vol. 108, pp. 131–137.

[19] AINLEY D.G., MATHIESON G.C.R., 1951: A Method for Performance Estimation of Axial-Flow Turbines, ARC R&M 2974.

[20] AINLEY D.G., MATHIESON G.C.R., 1951: An Examination of the Flow and Pressure Losses in Blade Rows of Axial-Flow Turbines, ARC R&M 2891.

[21] DUNHAM J., CAME P.M., 1970: Improvements to the Ainley-Mathieson Method of Turbine Performance Prediction, ASME Journal of Engineering for Power, July 1970.

[22] KACKER S.C., OKAPUU U., 1982: Mean line Prediction Method for Axial Flow Turbine Efficiency, ASME Journal of Engineering for Power vol. 104/1, pp 111–119.

[23] ZHU J., SJOLANDER S.A., 2005: Improved Profile Loss and Deviation Correlations for Axial-Turbine Blade Rows, Proceedings of ASME Turbo Expo 2005, paper GT2005-69077.

[24] BENNER M.W., SJOLANDER S.A., MOUSTAPHA S.H., 1997: Influence of Leading-Edge Geometry on Profile Losses in Turbines at Off-Design Incidence: Experimental Results and an Improved Correlation, ASME Journal of Turbomachinery, vol. 119, pp 193–200.

[25] BENNER M.W., SJOLANDER S.A., MOUSTAPHA S.H., 2005: An Empirical Prediction Method for Secondary Losses in Turbines: Part I – A New Loss Breakdown Scheme and Penetration Depth Correlation, Proceedings of ASME Turbo Expo 2005, paper GT2005-68637.

[26] BENNER M.W., SJOLANDER S.A., MOUSTAPHA S.H., 2005: An Empirical Prediction Method for Secondary Losses in Turbines: Part II – A New Secondary Loss Correlation, Proceedings of ASME Turbo Expo 2005, paper GT2005-68639.

[27] DUNHAM J., 1970: A Review of Cascade Data on Secondary Losses in Turbines, Journal of Mechanical Engineering Science, vol. 12/1, pp 48–59.

[28] STRATFORD, B.S., 1967: The Use of Boundary Layer Techniques to Calculate the Blockage from the Annulus Boundary Layers in a Compressor, ASME Paper 67-WA/GT-7.

[29] CRAIG H.R.M., COX H.J.A, 1970: Performance Estimation of Axial Flow Turbines, Proceedings of the Institution of Mechanical Engineers 1970-71, vol. 185 32/71, pp 407–424.

[30] WEI N., 2000: Significance of Loss Models in Aerothermodynamic Simulation for Axial Turbines, PhD Thesis, Royal Institute of Technology (KTH), Sweden.

[31] HIRSCH CH., 1988: Numerical Computation of Internal and External Flows - Volume 1: Fundamentals of Numerical Discretization, John Wiley & Sons, Chichester, UK.

[32] JENNIONS I.K., STOW P., 1985: A Quasi Three Dimensional Turbomachinery Blade Design System: Part 1 - Throughflow Analysis, ASME Journal of Engineering for Gas Turbines and Power, vol. 107, pp. 301–307.

[33] BARTH T.J., 1993: Recent Developments in High Order K-Exact Reconstruction on Unstructured Meshes, AIAA Paper 93–0668.

[34] HORLOCK J.H., PERKINS H.J., 1974: Annulus Wall Boundary Layers in Turbomachines, AGARD Lecture Series AG-185.

[35] BURDSALL E.A., CANAL E.Jr, LYONS K.A., 1979: Core Compressor Exit Stage Study-I. Aerodynamic and Me-

chanical Design, NASA Contract Report CR-159714.

[36] BEHLKE R.F., BURDSALL E.A., CANAL E.Jr, KORN N.D., 1980: Core Compressor Exit Stage Study - II. Final Report, NASA Contract Report CR-159812.

[37] TIMKO L.P., 1984: Energy Efficient Engine High Pressure Turbine Component Test Performance Report, NASA Contract Report 168289.

[38] RODRIGUEZ C.G., 1997: One-Dimensional, Finite-Rate Model for Gas-Turbine Combustors, Ph.D. Thesis, Virginia Polytechnic Institute and State University, USA.

[39] HARTSEL J.E., 1972: Prediction of Effects of Mass-Transfer Cooling on the Blade Row Efficiency of Turbine Airfoils, AIAA Paper 72–11.

[40] ITO S., ECKERT E.R.G., GOLDSTEIN R.J., 1980: Aerodynamic Loss in a Gas Turbine Stage with Film Cooling, ASME Journal of Engineering for Power, vol. 102, pp 964–970.

[41] AUNGIER R.H., 2000: Centrifugal Compressors: a Strategy for Aerodynamic Design and Analysis, ASME Press, New York.

[42] VON BACKSTRÖM T.W., 2006: A Unified Correlation for Slip Factors in Centrifugal Impellers, ASME Journal of Turbomachinery, vol. 128, pp 1–10.